A Topological Approach to Path Planning for a Magnetic Millirobot

Ariella Mansfield[1], Dhanushka Kularatne[1], Edward Steager[1], and M. Ani Hsieh[1]

Abstract— **We present a path planning strategy for a magnetic millirobot where the nonlinearities in the external magnetic force field (MFF) are encoded in the graph used for planning. The strategy creates a library of candidate MFFs and characterizes their topologies by identifying the unstable manifolds in the workspace. The path planning problem is then posed as a graph search problem where the computed path consists of a sequence of unstable manifold segments and their associated MFFs. By tracking the robot's position and sequentially applying the MFFs, the robot navigates along each unstable manifold until it reaches the goal. We discuss the theoretical guarantees of the proposed strategy and experimentally validate the strategy.**

I. INTRODUCTION

For actuation of small-scale robotic systems, magnetic control methods have garnered significant interest since magnetic fields can be selectively applied without affecting non-magnetic materials [1]–[3]. This is particularly useful when working with biological cells and tissues [4]. Existing approaches in magnetic control of single and multiple microrobots have mostly focused on two aspects of the problem: 1) design of the physical geometry of the robot, and 2) design of devices to manipulate the local magnetic field. In both cases, the focus is on the local forces that the magnetic field can exert on the robot, rather than the global topology of the resulting force field. And yet, existing work in controlling autonomous vehicles in fluid flows have shown that the vector field topology can be leveraged for planning energy efficient trajectories [5]–[7], maintaining sensors in the desired monitoring regions [8]–[10], and for diagnosing the underlying dynamics of the system.

These results build upon the recent synthesis of ideas from nonlinear dynamics and fluid dynamics to develop the concept of Lagrangian coherent structures (LCS), which provides a new way of understanding transport. In general, LCS provide a method to identify key material lines that organize transport in a flow. For time-independent, periodic, or quasi-periodic flows, there exists a well-known and detailed understanding of transport that is based on having knowledge of critical points and stable or unstable manifolds. However, for aperiodic flows, one must rely on the modern characterization using LCS [11]. Critical points, stable/unstable manifolds, and their time varying counterparts – LCS, can also be used to understand transport in magnetic fields since, as in fluid flows, these topological structures separate the phase space into regions where the magnetic fields result in different types of motion [12].

Previous work has shown that it is possible to utilize the spatially varying gradients of the magnetic field to manipulate microrobots along dynamically distinct trajectories in 2-D [13], and in 3-D [14]. In [13] a global field is generated by four stationary electromagnetic coils placed with the coils perpendicular to the plane. Using the spatially varying magnetic field gradients close to the coil and linearly superimposing the magnetic fields, different forces were applied on identical magnets at close proximity by mapping forces exerted on the robots to the coil input currents. Different from previously existing magnetic control techniques, [13] took advantage of the spatial variations in the magnetic force field generated by the four stationary coils by varying the currents through the coils. Thus, it enabled the trajectories to be executed simultaneously without the need to introduce additional complexity in the form of heterogeneous robots, *i.e.*, robots of different shapes and/or magnetization, or a specialized substrate.

While [13] did not explicitly address the global topology of the total magnetic force fields used to actuate the microrobots, the approach effectively leveraged the inherent nonlinearities of the field. In this work, we present a method for constructing a graph that connects topological features of the external magnetic force fields. We show how this graph can be used in a path planning and trajectory following strategy for millimeter and micro scale robots. A significant advantage of leveraging topological features of the force vector field is that it does not require complete knowledge of the field and yet results in comparable performance to vehicles following optimal paths where the vector field has been explicitly accounted for [5]. To the author's knowledge, this is one of the first attempts to employ knowledge of magnetic force field topology in designing more effective magnetic control strategies for microrobot applications.

The rest of the paper is organized as follows: We provide some background and formulate the problem in Section II. The proposed methodology is presented in Section III and its theoretical properties are analyzed in Section IV. Experimental validation of the strategy is presented in Section V and discussed in Section VI. A brief discussion of directions for future work is presented in Section VII.

II. PROBLEM FORMULATION

A. Background

We are interested in developing motion and path planning strategies for millimeter and micron scale robots that

This work was supported by the National Science Foundation (NSF) grants CMMI 1462825 and 1760369.

[1]The authors are with the General Robotics, Automation, Sensing, and Perception (GRASP) Laboratory at the University of Pennsylvania, Philadelphia, Pennsylvania 19104, USA {ariellam,dkul,esteager,m.hsieh}@seas.upenn.edu

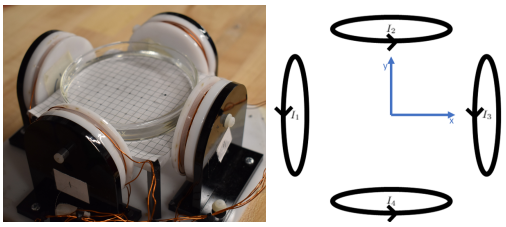

(a) (b)

Fig. 1: (a) Experimental setup used to generate magnetic fields by running currents through 4 coils. (b) Schematic representation of the setup.

leverages the inherent nonlinearities in the external magnetic fields used to actuate them. A ferromagnetic particle with a magnetic dipole $\mathbf{m}$ placed in a magnetic field $\mathbf{B}$ will experience a magnetic force and torque given by:

$$\mathbf{F_B} = (\mathbf{m}\cdot\nabla)\mathbf{B}, \tag{1a}$$

$$\tau = \mathbf{m}\times\mathbf{B}. \tag{1b}$$

In general $\mathbf{m}$ depends on the material properties and the geometry of the particle.

In this work, we assume the magnetic field is generated by N stationary electromagnetic coils placed with the coils perpendicular to a planar workspace as shown in Fig. 1. The magnetic field generated at a point in space by a current running through a wire is given by the Biot Savart equation:

$$\mathbf{B}(\mathbf{L},I) = \frac{\mu_0 I}{4\pi}\int_C \frac{d\mathbf{s}\times\hat{\mathbf{L}}}{L^2} \tag{2}$$

where $\int_C$ denotes the line integral over the current path C and $d\mathbf{s}$ denotes a differential coil segment vector in the direction of the positive current flow. The magnetic permeability of free space is denoted by μ_0, I is the current running through the coil, and L, $\hat{\mathbf{L}}$ are the distance and unit vector from $d\mathbf{s}$ to the point of interest, respectively.

To evaluate the contribution of each coil to the resultant magnetic field, consider the magnetic field generated by a single loop of wire with radius R such that the loop is parallel to the $y-z$ plane with the loop center located at $(0,0,0)$. Using (2), the contribution of this coil loop to the magnetic field is at a point $[x,y,0]^T$ is given by [15]:

$$\begin{aligned} B_x &= \frac{\mu_0 IR}{4\pi}\int_0^{2\pi}\frac{y\sin\phi' - R}{(R^2+y^2+x^2-2yR\sin\phi')^{1.5}}d\phi', \\ B_y &= -\frac{\mu_0 IRx}{4\pi}\int_0^{2\pi}\frac{\sin\phi'}{(R^2+y^2+x^2-2yR\sin\phi')^{1.5}}d\phi', \\ B_z &= 0. \end{aligned} \tag{3}$$

Thus, these expressions for the magnetic field are used to compute the force and torque, *e.g.*, (1), exerted on a robot (a permanent magnet) by a single coil in the workspace. The torque acts to align the dipole of the robot with the field, $\mathbf{B}$. In this model, we assume that this reorientation occurs immediately for the robot, and the robot is always torque free [16], [17]. Additionally, we assume assume that the effect of the applied magnet field on the magnetization of the robot is negligible.

Given the magnetic force on the magnetic object, the net force driving its motion can then be computed by summing all the contributions of the N coils. In this work we assume a linear drag law for resistive force. The magnetic force field (MFF) created by four stationary electromagnetic coils placed around a planar workspace similar to the one in Fig. 1 is shown in Fig. 2a. The stable and unstable manifolds for this field are highlighted in yellow in Fig. 2b.

The manifolds in Fig. 2b separate the phase space into regions where the MFF exhibits different types of behavior. This can be seen by examining the corresponding vector field shown in Fig. 2a. The saddle point at the location denoted by **P1** has associated stable and unstable manifolds which are respectively denoted by $\mathscr{M}_S$ and $\mathscr{M}_U$ in Fig. 2b. These manifolds partition the space into dynamically distinct regions. Thus, robots starting on opposite sides of these boundaries travel along dynamically distinct trajectories. By initiating robots at different positions in the workspace and switching between fields with different manifold arrangements, the nonlinearity and the topology of the global MFF can be leveraged to control single and possibly multiple microrobots in the workspace as shown in Figs. 2c - 2f.

In this example, both robots are initialized in a region of the workspace where the dynamics are consistent based on the arrangements of stable and unstable manifolds, *i.e.*, the MFF topology, regardless of the field. The field shown in Fig. 2c does not contain any critical points nor manifolds and thus applying this field would drive the robots towards the right side of the workspace. Similarly, for the same starting positions, if we apply the field shown in Fig. 2a, then both microrobots' starting position would be to the left of $\mathscr{M}_U$. Thus, if we only apply the field shown in Fig. 2e, the robots would remain to the left of $\mathscr{M}_U$ for all time. As such, the trajectories for the two microrobots shown in Fig. 2 would be infeasible if only one of the fields is used to drive the microrobots. By sequentially applying one field after the next, the robots are thus able to reach a portion of the workspace that would otherwise be inaccessible had only one field been used. The idea of sequentially switching the external magnetic fields to control the motions of active microrobots has been shown in [18]. However, [18] only switched between spatially uniform fields and thus did no consider nor utilize the topology of the field.

Unfortunately, the identification of critical points, manifolds, or LCS can only be achieved analytically or through global knowledge of the vector field. Fortunately, a variety of numerical techniques have been developed to find unstable and stable manifolds and LCS for a wide range of dynamical systems. Some of these techniques include the Principle Interior Maximum (PIM) triple procedure for chaotic systems [19], Finite Time Lyapunov Exponents (FTLE) for LCS [20]. We refer the interested reader to [21] for a broad survey of existing techniques. In this work, we propose a path planning strategy for magnetically actuated microrobots that leverages sequential switching between time-invariant MFFs of varying topologies. Thus, our approach will focus on the leveraging the manifolds in static MFFs rather than LCS in time-varying

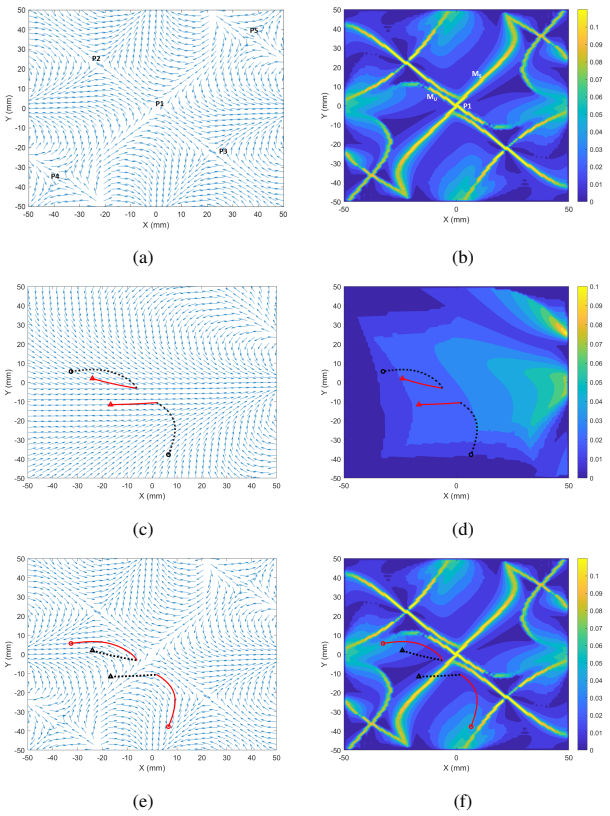

Fig. 2: (a) Vector field and (b) stable and unstable manifolds of a magnetic field generated using four inward-facing electromagnetic coils with equal currents. (c)-(f) Example of two robot trajectories with the starting positions denoted by a △ and end positions denoted by ◯. These trajectories were obtained by applying the force field shown in (c) whose manifolds are shown in (d) for 19 seconds, followed by applying the force field shown in (e) whose manifolds are shown in (f) for 30 seconds. The portion of the trajectories resulting from the background field is shown in solid red and the portion resulting from the other field is shown in dashed black. The stable and unstable manifolds were obtained through the computation of finite time Lypunov exponents (FTLEs) [20] and are highlighted in in yellow.

MFFs.

B. Problem Statement

Let Q denote the configuration space of the microrobot with $\mathbf{q}_s$ and $\mathbf{q}_g$ denoting the robot's desired initial and final configurations. The kinematics of a ferromagnetic microrobot operating in a planar fluid workspace surrounded by N electromagnetic coils mounted perpendicular to the workspace is given by:

$$\dot{\mathbf{q}} = \alpha \nabla \Big(||\mathbf{B}(\mathbf{q}, \mathbf{I})|| \Big) \tag{4}$$

where α is a constant related to the magnetic dipole moment, the millirobot mass, and the Stokes drag. Note that $\mathbf{B}$ is the resultant magnetic field where the contributions from each coil is given in (3). In this work, we assume the robot aligns with the magnetic field instantaneously and the robot is always torque free. This assumption is reasonable when the time it takes the robot to align with the field is negligible relative to the time it takes the robot to execute the trajectory. Furthermore, at the millimeter and micron scales, robots effectively operate in a low Reynolds regime and thus the robot velocity is assumed to be proportional to the actuating force [22]. Given these assumptions, the robot kinematics are effectively holonomic. Coupled with the fact that $\mathbf{B}_i$ from each coil is linear in I, we note that the robot experiences the same velocity for both positive and negative current values. This is true as long as the effects of other external fields, *e.g.* Earth, are negligible relative to the generated field.

Let $U = \{\mathbf{I}_1, \ldots, \mathbf{I}_K\}$ denote the discrete set of K feasible input currents that generates the set of MFFs to actuate the robot for an N coil system. In general, K depends on N and is chosen such that for every $i, j \in \{1, \ldots, K\}$ the topologies of the i^{th} and j^{th} MFFs are sufficiently distinct. Then the path and trajectory planning problem for the microbot can be mathematically stated as follows:

$$\begin{aligned} \boldsymbol{\tau}_{\mathbf{u}}{}^* = \underset{\boldsymbol{\tau}_{\mathbf{u}}}{\operatorname{argmin}} & \int_{t_s}^{t_g} C(\boldsymbol{\tau}_{\mathbf{u}}(t), t) dt \\ \text{s.t.} \quad & \dot{\mathbf{q}} = \alpha \nabla \Big(||\mathbf{B}(\mathbf{q}, \mathbf{u})|| \Big) \\ & \boldsymbol{\tau}_{\mathbf{u}}(\mathbf{q}_s, t_s) = \mathbf{q}_s \\ & \boldsymbol{\tau}_{\mathbf{u}}(\mathbf{q}_s, t_g) = \mathbf{q}_g \\ & \boldsymbol{\tau}_{\mathbf{u}}(\mathbf{q}_s, t) \in Q, \forall t \in [t_s, t_g] \\ & t_g \in [t_s, \infty) \end{aligned} \tag{5}$$

where $C(\boldsymbol{\tau}_{\mathbf{u}}(t), t)dt > 0$ can denote path length, energy expenditure, and/or travel time. The solution to this optimization problem should yield a MFF switching strategy that consists of an ordered sequence of feasible input currents when applied would drive the robot from the initial to the final desired configurations.

III. METHODOLOGY

The objective is to develop a path planning algorithm that leverages the nonlinearities in the controlled kinematic field of the robot. We accomplish this by first identifying the unstable manifolds in each MFF generated by every element in U. The path planning problem is then formulated as a graph search problem where the vertices represent intersections between manifolds in different MFFs and edges denote trajectories along candidate manifolds that the robot traverse to move from one intersection point to another. We describe our methodology in detail below.

A. Planning Paths Along Unstable Manifolds

We begin by identifying the unstable manifolds, if they exist, of the MFFs generated by a set of predetermined input currents given by U. Given a saddle point in the field, the unstable manifold of the saddle point is given by the direction of instability of the local linear approximation of the field dynamics around the point. A passive particle originating within a small neighborhood of a saddle point, will move away from the saddle point locally exponentially fast and approach the unstable manifold as it moves away from the saddle point. Thus, trajectories along unstable manifolds are locally attracting by nature as illustrated in Fig. 2a. The basin of attraction refers to the local attracting neighborhood

around the unstable manifold. As long as the robots stay within this basin of attraction, they will always converge onto a trajectory which corresponds to an unstable manifold.

Our ability to generate a path from arbitrarily chosen start and goal locations in the workspace depends on how densely our workspace can be covered by unstable manifolds for a given set of U and their associated MFFs. A sparsely covered workspace will be more limited in the set of reachable configurations. Coverage thus is a function of N, the number of coils used, their arrangement around the workspace, and the input currents to the coils. By better understanding the topology of the available MFFs, the design of coil arrangements as well as the choice for K, number of feasible input currents, can be better determined. Fig. 3a provides a schematic on how coverage density of the workspace can be determined for a four coil arrangement. As such, we assume K is determined *a priori* and chosen to achieve some desired coverage density dictated by the particular application.

Given K, it is possible to create a roadmap for the workspace by looking at the intersections of all the manifolds extracted from each MFF created from the set of feasible input currents U. Let M denote the total number of unstable manifolds obtained from the feasible current set U. Fig. 3d shows the set of unstable manifolds extracted from a four coil arrangement similar to the one shown in Fig. 1 overlayed onto a $10cm \times 10cm$ workspace. The roadmap is then given by the graph $\mathscr{G} = (\mathscr{V}, \mathscr{E})$ such that the vertex set $\mathscr{V}$ is given by the intersection point(s) of any two unstable manifolds, $\mathscr{M}_i$ and $\mathscr{M}_j$, for any $i, j \in \{1, \ldots, M\}$. Then a directed edge $e_{kl} \in \mathscr{E}$ exists if the force along the manifold that connects $v_k, v_l \in \mathscr{V}$ moves a particle (or robot) from v_k to v_l. In general, given a set of feasible currents U, it is difficult to predict the size of $\mathscr{G}$ *a priori* without a thorough analysis of the MFF topologies. Nevertheless, once constructed, $\mathscr{G}$ serves as the roadmap for the workspace.

Given the roadmap $\mathscr{G}$ and a desired start and goal configurations, $\mathbf{q}_s, \mathbf{q}_g \in \mathscr{V}$, any graph search methodology, *e.g.* Dijkstra's or A*, can be used to find the optimal path. In situations when $\mathbf{q}_s, \mathbf{q}_g \notin \mathscr{V}$ but are located directly on a manifold in $\mathscr{M}$, $\mathscr{G}$ can be expanded by adding the points $\mathbf{q}_s$ and $\mathbf{q}_g$ to $\mathscr{V}$ and their corresponding edges to $\mathscr{E}$. When $\mathbf{q}_s, \mathbf{q}_g$ are not on any manifold in $\mathscr{M}$, let $\mathbf{q}'_s$ and $\mathbf{q}'_g$ denote the closest points to $\mathbf{q}_s$ and $\mathbf{q}_g$ respectively located on manifolds in $\mathscr{M}$. Then, $\mathscr{G}$ is expanded by adding the points $\mathbf{q}'_s$, $\mathbf{q}'_g$ to $\mathscr{V}$ and their corresponding edges to $\mathscr{E}$. The output of the search strategy would then consist of the set output currents $U_{pp} = \{\mathbf{I}_{k_1}, \ldots, \mathbf{I}_{k_P}\} \subset U$ where $k_i \in \{1, \ldots, K\}\ \forall i$ and their a sequence of manifolds $\mathscr{M}_{pp} = \{\mathscr{M}_{l_1}, \ldots, \mathscr{M}_{l_P}\}$ where $l_i \in \{1, \ldots, M\}\ \forall i$ that constitutes the robot's trajectory. It is important to note that $\mathscr{M}_{l_i}$ is a manifold that exists in the MFF generated by the input current $\mathbf{I}_{k_i}$ and thus $|U_{pp}| = |\mathscr{M}_{pp}|$. The procedure is summarized in Algorithm 1.

Algorithm 1: Path Planning Along Manifolds

Result: A path with P steps that is defined along manifolds $\{\mathscr{M}_{l_i}\}_{i=1}^{P}$ from start $\mathbf{q}_s$ to goal $\mathbf{q}_g$ and an associated discrete set of current inputs $\{\mathbf{I}_{k_i}\}_{i=1}^{P}$

given K sets of current inputs;
for $i \leftarrow 1$ **to** K **do**
    find unstable manifolds generate by $\mathbf{I}_i$;
    $\mathscr{V} \leftarrow$ add new intersections between manifolds;
    $\mathscr{E} \leftarrow$ add new edges
end
$\mathscr{G} = (\mathscr{V}, \mathscr{E})$;
graph search from $\mathbf{q}_s$ to $\mathbf{q}_g$ (e.g. Dijkstra's, A^*) outputs a path with P steps

B. Trajectory Following

To enable the robot to follow the output path given by Algorithm 1, the set of input currents U_{pp} are applied sequentially. For every $\mathbf{I}_{k_i} \in U_{pp}$ applied, the robot should travel along the corresponding $\mathscr{M}_{l_i} \in \mathscr{M}_{pp}$. As robots move along $\mathscr{M}_{l_i}$, position feedback control is used to determine when to switch the current input signal from $\mathbf{I}_{k_i}$ to $\mathbf{I}_{k_{i+1}}$ so the robot can move along $\mathscr{M}_{l_{i+1}}$. To allow robots to move continuously from one manifold to the next, switching occurs when robots are within some neighborhood of $\mathscr{M}_{k_{i+1}}$ as it moves along $\mathscr{M}_{k_i}$. Let p denote a point on the manifold $\mathscr{M}_{l_i}$ such that $\mathscr{B}_p$ denotes an open ball centered around p. We define the neighborhood of $\mathscr{M}_{l_i}$ as the open set $\mathscr{N}_{l_i} \triangleq \{\cup \mathscr{B}_p \forall p \in \mathscr{M}_{l_i} | \|p - p^c_{l_i}\| > \delta\}$ where $p^c_{l_i}$ is a critical point on $\mathscr{M}_{l_i}$. In other words, the neighborhood of $\mathscr{M}_{l_i}$ effectively forms a tube around $\mathscr{M}_{l_i}$ that does not include the region around the critical points on $\mathscr{M}_{l_i}$. For any robot $\mathbf{q} \in \mathscr{N}_{l_i}$, the following is true:

a) The robot is in the basin of attraction of manifold $\mathscr{M}_{l_i}$ of the MFF generated by $\mathbf{I}_{k_i}$ as long as the radius $\mathscr{B}_p$ is chosen to be large enough; and
b) The trajectories of points originating in $\mathscr{N}_{l_i}$ before the next manifold $\mathscr{M}_{l_{i+1}}$ will intersect with the next manifold $\mathscr{M}_{l_{i+1}}$ in the set $\mathscr{M}_{pp}$.

To ensure robots successfully switch from one manifold to the next, we require that switch between successive $\mathbf{I}_{k_i}$'s in U_{pp} satisfy the following criteria:

(i) It occurs before the robot's trajectory in $\mathscr{N}_{l_i}$ intersects the next manifold $\mathscr{M}_{l_{i+1}}$.
(ii) If $i = l_p$, *i.e.*, the robot is moving along the last manifold in $\mathscr{M}_{pp}$, the input current is set to $\mathbf{0}$ once the robot is within an ε-neighborhood of $\mathbf{q}_g$.

Condition (i) ensures the robot does not cross the next manifold as it moves along its current manifold. This ensures that robots are always traveling in a direction such that they converge onto the path given by $\mathscr{M}_{pp}$. Condition (ii) ensures that the robot stops within some $\varepsilon > 0$ distance from the goal location. In practice, switching between input currents occurs when $D(\mathbf{q}, \mathscr{M}_{l_{i+1}}) < \delta$ where $D(;)$ denotes the straight line distance and $\delta > 0$ is a suitably small constant. A schematic of these conditions are shown in Fig. 4a for some candidate set of manifolds. The trajectory following algorithm is given by Algorithm 2.

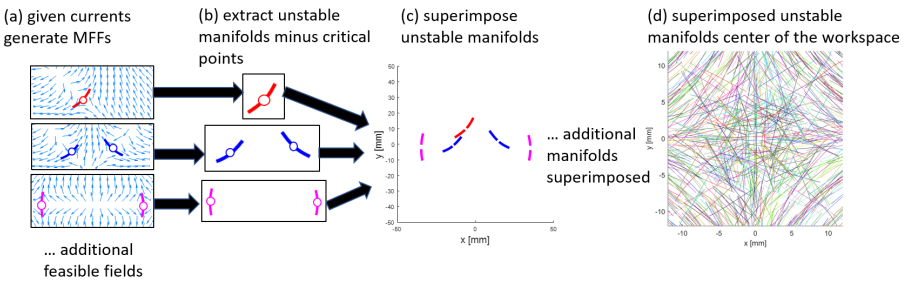

Fig. 3: The graph of superimposed unstable manifolds is generated by: (a) modeling the MFF for each current set in U. (b) extracting the unstable manifolds from each field. (c) superimposing these manifolds all together. (d) Zoomed in view after many manifolds have been extracted. The intersections of the superimposed manifolds become vertices $\mathscr{V}$ and the connections between them become directed edges $\mathscr{E}$.

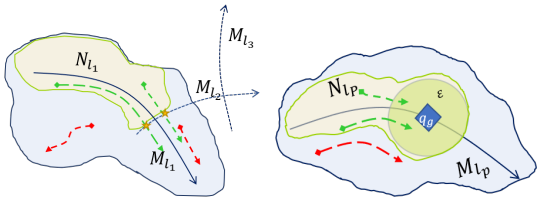

Fig. 4: (a) Illustration of a neighborhood N_{l_1} (in orange) before it intersects with the next manifold $\mathscr{M}_{l_2}$. Trajectories in green show how robots will converge onto the path (by switching currents to $\mathbf{I}_{k_2}$ when they reach the intersections denoted with a star). (b) In the last neighborhood $\mathscr{N}_{l_P}$ the robot reaches an ε-neighborhood (in green) from the goal (blue diamond).

If the robot leaves the neighborhood $\mathscr{N}_{l_i}$ of the manifold it is following, Algorithm 2 is not guaranteed to hold. In this case, Algorithm 1 can be used to calculate a new path from the current location to the goal.

Remark 1: By leveraging the topology of the MFFs, the proposed planner is agnostic to the dipole moment, at least under the assumption that inertia is negligible.

Remark 2: Since changes in the current input are based on the robot's position, position feedback control can occur at a relatively slow rate relatively to the robot's speed. As long as the robot stays within $\mathscr{N}_{l_i}$ as it moves along $\mathscr{M}_{l_i}$ and reaches $\mathscr{N}_{l_{i+1}}$, then the computed path remains valid.

Remark 3: In situations where $\mathbf{q}_s$ and/or $\mathbf{q}_g$ are not on any manifold in $\mathscr{M}$ and are outside the region of attraction of $\mathscr{M}_{l_1}$, $\mathscr{M}_{l_P}$ respectively, it is possible to append an initial and/or final input current, $\mathbf{I}_s$, $\mathbf{I}_g$, to the set U_{pp} such that the MFFs associated with $\mathbf{I}_s$, $\mathbf{I}_g$ drives the robot towards the $\mathscr{N}_{l_1}$ and an ε-neighborhood of $\mathbf{q}_g$ respectively. Since these distances are generally small, especially when coverage density for the workspace is high, $\mathbf{I}_s$, $\mathbf{I}_g$ can be determined relatively easily.

IV. ANALYSIS

We present the theoretical properties of our proposed path planning and trajectory following strategy.

Theorem 1: Given $\mathscr{G} = (\mathscr{V}, \mathscr{E})$, U_{pp}, and $\mathscr{M}_{pp}$, for any $\mathbf{q}_s$ and $\mathbf{q}_g$ such that $\mathbf{q}_s, \mathbf{q}_g \in \mathscr{V}$, Algorithm 2 will drive a robot to within an ε-neighborhood of $\mathbf{q}_g$.

Proof: We will prove this by induction. Let $\mathbf{q}(n)$ denote the robot's position at the n^{th} iteration of Algorithm 2.

Algorithm 2: Executing Planned Path

Result: Robot follows trajectory planned from start $\mathbf{q}_s$ to goal $\mathbf{q}_g$

use Algorithm 1 to obtain P discrete sets of currents $\{\mathbf{I}_{k_i}\}_{i=1}^{P}$ to follow and corresponding manifolds $\{\mathscr{M}_{l_i}\}_{i=1}^{P}$ along which the robot will travel ;
initial robot location $\mathbf{q} = \mathbf{q}_s$;
i=1;
while Condition (ii): $||\mathbf{q} - \mathbf{q_g}|| > \varepsilon$ **do**
    apply currents $\mathbf{I}_{k_i}$;
    if $i < P \wedge$ Condition (i): $\mathbf{q} \in \mathscr{N}_{l_i} \wedge$ before $\mathscr{M}_{l_{i+1}}$ **then**
        i=i+1
    end
end

For the base case with $n = 1$ and $\mathbf{q}(1) \in \mathscr{N}_{l_1}$, the applied current is given by $\mathbf{I}_{k_1}$. Thus the robot's trajectory converges towards $\mathscr{M}_{l_1}$ and will intersect with $\mathscr{M}_{l_2}$. Furthermore, we only switch from $\mathbf{I}_{k_1}$ to $\mathbf{I}_{k_2}$ when the robot enters the region given by $\mathscr{N}_{l_1} \cap \mathscr{N}_{l_2}$ but before the robot crosses $\mathscr{M}_{l_2}$. Thus, $n = 1$, the robot converges towards $\mathscr{M}_{l_1}$ as it moves in the direction of the intersection of $\mathscr{M}_{l_1}$ and $\mathscr{M}_{l_2}$.

Suppose the theorem holds for all values of n up to some $p \geq 1$. Then for the inductive step, let $n = p+1$. Then $\mathbf{q}(p+1) \in \mathscr{N}_{l_{p+1}}$ and the applied current is given by $\mathbf{I}_{k_{p+1}}$. Thus, the robot's trajectory converges towards $\mathscr{M}_{l_{p+1}}$ and will intersect with $\mathscr{M}_{l_{p+2}}$. Switching from $\mathbf{I}_{k_{p+1}}$ to $\mathbf{I}_{k_{p+2}}$ when the robot enters $\mathscr{N}_{l_{p+1}} \cap \mathscr{N}_{l_{p+2}}$ but before the robot crosses $\mathscr{M}_{l_{p+2}}$. Thus, the robot converges towards $\mathscr{M}_{l_{p+1}}$ and moves towards the intersection of $\mathscr{M}_{l_{p+1}}$ and $\mathscr{M}_{l_{p+2}}$. If $n = P$, then the algorithm stops and the current is set to $\mathbf{0}$ when $\|\mathbf{q}(P) - \mathbf{q}_g\| < \varepsilon$ for some $\varepsilon > 0$. ■

V. EXPERIMENTS

A. Setup

We validated our results using the 4 coil configuration shown in Fig. 1a. The coils are made of 22 gauge insulated copper wire, wrapped 40 times around an acrylic core with an inner diameter of 51 mm. Current through the coils is

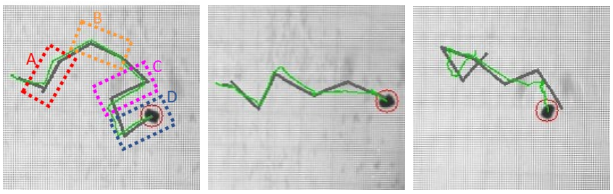

(a) (b) (c)

Fig. 5: Example trajectories shown on zoomed in views of video images. Dark grey lines represent the reference trajectory, the actual trajectory followed is shown in green, and the current position of the robot is circled in red. Highlighted portions from (a) shown in Fig. 6. Trajectories: (a) $[-9.0,-0.5] \rightarrow [12.2,-5.8]$mm (b) $[-3.1,-1.5] \rightarrow [22.6,-3.0]$mm (c) $[-2.5,-1.4] \rightarrow [8.8,-10.0]$mm.

provided by a power source and controlled using a computer via a digital-to-analog converter (DAC). An overhead camera and the OpenCV library [23] is used to track the position of the robot in the workspace.

Robots are cut from a ferrite sheet with dimensions of 1.6×2 mm. We magnetized the robots using a neodymium permanent magnet. They are actuated by the magnetic field generated from the currents in the surrounding coils. In this work, we include Earth's magnetic field, which adds a spatially constant offset to the fields generated by the coils. Thus, the total magnetic field experienced by the robot is given by:

$$\mathbf{B}(x,y,I_1,I_2,I_3,I_4) = \sum_{i=1}^{4} \mathbf{B}_i(x,y,I_i) + \mathbf{B}_{earth}. \qquad (6)$$

The planar workspace consists of a 93.5 mm diameter petri dish filled with water. As mentioned in Section III, our path planning and trajectory following strategy is agnostic to the dipole moment. While dipole moment influences the speed at which the robot traverses the manifolds, it does not impact our algorithm or solution. Thus, the robot's dipole moment was not computed.

In our experiments, the set U was obtained by considering input values between -0.7 A and 0.7 A for each current, with a total of $|U| = 687$ sets of currents. Since measuring the entire MFF is difficult, we computed the MFF for each set of candidate values of $\mathbf{I}_i$ using (3) and (4). The magnitude of Earth's magnetic field was obtained empirically and added to each MFF. The set of unstable manifolds in the workspace were then extracted numerically for each candidate MFF. This resulted in 1454 elements in $\mathscr{M}$. Fig. 3d shows the unstable manifolds for all the fields generated by currents in U superimposed on the center region of the workspace.

B. Results

Various paths obtained using Algorithm 1 were experimentally validated using Algorithm 2 to follow the computed paths. We required that paths did not have switches that were too close together and that the angle between subsequent manifolds was sufficiently large to allow the robot to practically follow the path. These conditions could be added as formal constraints to the optimization problem, if desired.

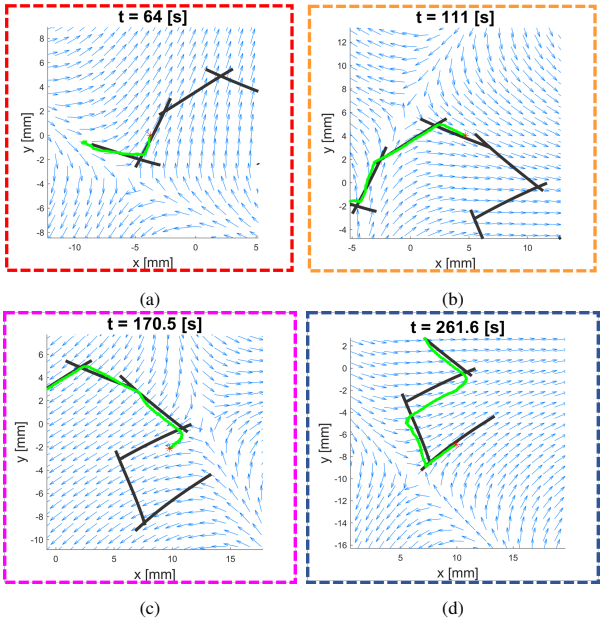

(a) (b) (c) (d)

Fig. 6: Zoomed in view of trajectory at different steps along the path shown in Fig. 5a, outline colors correspond to highlighted portions there. Black lines represent $\mathscr{M}_{pp}$. The actual trajectory followed is shown in green. Robot location is shown with a red $*$. Arrows indicate the MFF. (a) $\mathbf{I} = [-0.35,-0.7,0.35,0.35]A$, (b) $\mathbf{I} = [0.35,-0.35,-0.7,0]A$, (c) $\mathbf{I} = [0.7,0,-0.35,-0.7]A$, (d) $\mathbf{I} = [0,0,-0.35,-0.35]A$

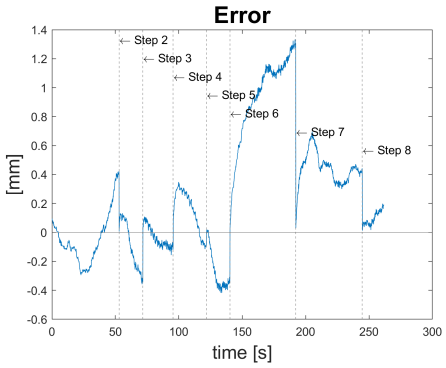

Fig. 7: Error along the trajectory shown in Fig. 5a. The error is measured as the distance from the current manifold that the robot is following. Negative values correspond to robot distance on the other side of the manifold.

Three example paths are shown in Fig. 5. The path shown in Fig. 5a consists of 8 distinct manifolds obtained from a total of 7 switches. Fig. 6 shows the robot's trajectory, the previous, current, and next manifolds in the robot's path, and the current MFF used to actuate the robot for 4 different time instances.

Fig. 5c shows an example where the robot follows a path that contains a cycle. We include this example to show a feature of the proposed methodology even though the path may not be an optimal path as stated in our problem statement.

Lastly, Fig. 7 shows error between the robot's position and the closest point on the manifold the robot is currently following over the course of a run. The error was computed using the robot's position and the manifold numerically

extracted from the computed MFFs. We note that any errors accumulated due to noise or model errors zeros out every time the input current switches and the robot starts following a new manifold. This is a significant advantage of the topological approach since robots switch between locally attracting neighborhoods of the manifolds as they traverse their paths.

VI. DISCUSSION

In general, it is difficult to provide a quantitative comparison between the proposed strategy and existing approaches since existing strategies do not address the topology of the MFF. Nevertheless, we consider a qualitative comparison between the proposed strategy and the one presented in [13] since Wong *et al.* explicitly used the spatial variations in the MFFs to achieve simultaneous control of multiple microrobots.

In [13], different forces were applied on identical magnets at close proximity by mapping forces exerted on the robots to the coil input currents. To enable the robots to follow the desired trajectories, the map is inverted to solve for the currents required to exert the desired force given the robot positions. This inverse mapping cannot be derived explicitly as the force does not depend linearly on the position or on the current (since the orientation of the robot's magnetic dipole is also a function of the current). The desired force is calculated using a feedback control strategy that changes depending on the robot's current and desired position, velocity and acceleration. Much of the complexity of the strategy described in [13] was the need to solve the inverse dynamics problem at waypoints along the planned path which often yield multiple solutions, *i.e.*, input current values for the four different coils. These challenges arose specifically because the approach did not explicitly consider the topology of the MFF.

Different from [13], this work examines the topology of the MFFs and developed a path planning strategy that leverages the inherent dynamics around unstable manifolds in the various MFFs. The approach circumvents the need to solve the inverse dynamics problem and the need to select among multiple possible solutions. The proposed planner is also agnostic to the robot's magnetic dipole moment and thus can be used whenever the torque free assumption on the robot holds. By leveraging the topology of the MFFs, the strategy is more robust to uncertainties that may arise from noisy position estimates or inaccurate model parameters as evidenced from our results. While the proposed strategy requires the predetermination of the a candidate set of inputs U and the extraction of the manifolds for all possible MFFs, these computations are done *a priori* and significantly limits the complexity of the strategy at run-time. Finally, the performance of the proposed strategy deteriorates when dust or dirt are present in the fluid, but this is not surprising since the planner was developed assuming an obstacle free workspace and the presence of such particulates invalidates that assumption. Nevertheless, the proposed planning strategy can be easily extended to environments with obstacles as long as the obstacles can be suitably localized.

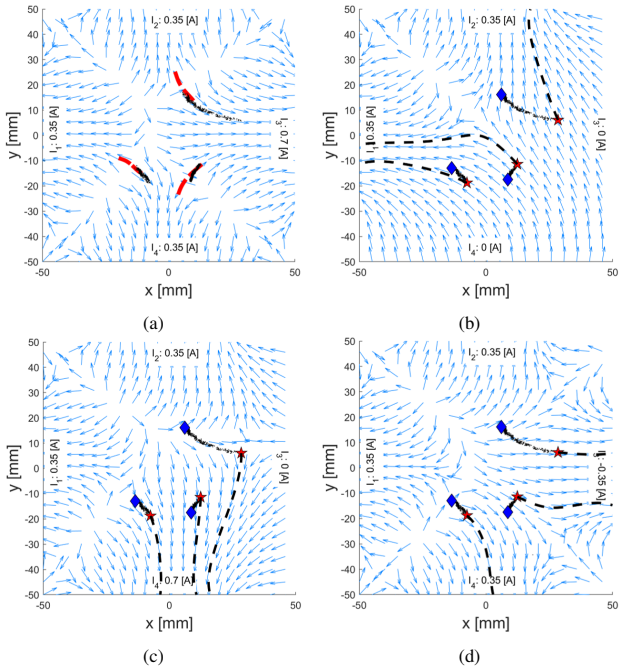

Fig. 8: (a) Three robots are placed near different manifolds of a field where $I = [0.35, 0.35, 0.7, 0.35]$A. Manifolds shown in red, arrows denote MFF, and robots' trajectories shown by black data-points. (b)-(d) Applying different subsequent currents can lead to significantly different results. Red star shows robot location at the end of the previous current set. Dashed line shows subsequent trajectory.

VII. FUTURE WORK

We present a path planning and trajectory following algorithm that leverages the inherent nonlinearities in the external magnetic force field (MFF) to navigate a millirobot from one desired configuration to another in an obstacle-free workspace. By identifying all the unstable manifolds in a set of predetermined candidate MFFs, the path planning problem can be posed as a graph search problem. The planned path is then a sequence of current inputs such that when applied sequentially enables the robot to travel along an unstable manifold in each of the generated MFFs. Switching is accomplished by tracking the robot's position as it moves along its path and occurs when the robot reaches the neighborhood of the intersection point between the current and next manifold on the path. We prove how the proposed strategy can guarantee the arrival of the robot at the desired final configuration given our assumptions. We experimentally validate the proposed strategy and discussed its advantages.

One direction of immediate future work is to consider how the global topology of the MFFs can be leveraged to achieve simultaneous control of multiple robots along dynamically distinct trajectories. Consider the placement of two robots on opposite of a *stable manifold*. Stable manifolds are along the directions of local attraction in a small enough neighborhood of a saddle point. Particles moving on opposite sides of the stable manifold are locally repelled away from the manifold itself. Similarly, particles will be attracted towards *unstable manifolds*. In each MFF, we can then use these stable and

unstable manifolds as repellers and attractors in the field. Thus, by strategically placing multiple robots in distinct initial configurations, coupled with switching between distinct MFFs, it is possible to achieve simultaneous control and navigate the team along vastly distinct trajectories and paths. Consider the example shown in Fig. 8 where three robots are positioned in the field such that each follows a different unstable manifold (Fig. 8a). Fig. 8b-8d show three different sets of paths resulting from the application of three distinct sets of input currents. While the addition of multiple robots would significant complicate the search problem, nevertheless by leveraging the topology of the MFFs it may be possible to achieve more complex collective behaviors, *e.g.*, aggregation, pattern formation, especially as the size of the robots are scaled down.

Another interesting direction for future work is to develop continuous paths for robots to follow along manifolds. Instead of following a discrete set of unstable manifolds in MFFs, we would be interested in investigating methods to gradually change the placement of the manifolds. Gradual changes of the manifolds would enable smoother paths and perhaps allow for greater control of the robot trajectory.

REFERENCES

[1] M. P. Kummer, J. J. Abbott, B. E. Kratochvil, R. Borer, A. Sengul, and B. J. Nelson, "Octomag: An electromagnetic system for 5-dof wireless micromanipulation," IEEE Trans. on Robotics, vol. 26, no. 6, pp. 1006–1017, 2010.

[2] C. Pawashe, S. Floyd, and M. Sitti, "Modeling and Experimental Characterization of an Untethered Magnetic Micro-Robot," Intl. J. of Robotics Research, vol. 28, no. 8, pp. 1077–1094, Jul. 2009.

[3] W. Jing, X. Chen, S. Lyttle, Z. Fu, Y. Shi, and D. J. Cappelleri, "Design of a micro-scale magnetostrictive asymmetric thin film bimorph (μmab) microrobot," in ASME 2010 International Mechanical Engineering Congress and Exposition, 2010, pp. 599–607.

[4] E. B. Steager, M. S. Sakar, C. Magee, M. Kennedy, A. Cowley, and V. Kumar, "Automated biomanipulation of single cells using magnetic microrobots," Intl. J. of Robotics Research, vol. 32, no. 3, pp. 346–359, 2013.

[5] T. Inanc, S. Shadden, and J. Marsden, "Optimal trajectory generation in ocean flows," in Proceedings of the 2005 American Control Conference, 8-10 2005, pp. 674 – 679.

[6] D. Kularatne and M. A. Hsieh, "Tracking attracting lagrangian coherent structures in flows," in Proceedings of Robotics: Science and Systems, Rome, Italy, July 2015.

[7] D. Kularatne, S. Bhattacharya, and M. A. Hsieh, "Time and energy optimal path planning on a flow field," in submitted to Robotics: Science and Systems, Ann Arbor, MI USA, May 2016.

[8] C. R. Heckman, M. A. Hsieh, and I. B. Schwartz, "Controlling basin breakout for robots operating in uncertain flow environments," in International Symposium on Experimental Robotics (ISER 2014), Marrakech/Essaouira, Morocco, June 2014.

[9] D. Kularatne, E. Forgoston, and M. A. Hsieh, "Exploiting stochasticity for the control of transitions in gyre flows," in Proceedings of Robotics: Science and Systems, Pittsburgh, Pennsylvania, June 2018.

[10] ——, "Using control to shape stochastic escape and switching dynamics," Chaos: An Interdisciplinary Journal of Nonlinear Science, vol. 29, no. 5, p. 053128, 2019.

[11] T. Peacock and G. Haller, "Lagrangian coherent structures: The hidden skeleton of fluid flows," Physics Today, vol. 66, no. 2, p. 41, 2013.

[12] G. Di Giannatale, M. Falessi, D. Grasso, F. Pegoraro, and T. Schep, "Coherent transport structures in magnetized plasmas. I. Theory," Physics of Plasmas, vol. 25, no. 5, p. 052306, 2018.

[13] D. Wong, E. B. Steager, and V. Kumar, "Independent control of identical magnetic robots in a plane," Robotics and Automation Letters, vol. 1, no. 1, pp. 554–561, 2016.

[14] F. Ongaro, S. Pane, S. Scheggi, and S. Misra, "Design of an electromagnetic setup for independent three-dimensional control of pairs of identical and nonidentical microrobots," IEEE transactions on robotics, vol. 35, no. 1, pp. 174–183, 2019.

[15] J. Belcher, P. Dourmashkin, S.-B. Liao, S.-I. Liao, C. Watkins, and E. Hudson. (2007, Spring) Physics II: Electricity and magnetism. Massachusetts Institute of Technology: MIT OpenCourseWare. [Accessed April-2019]. [Online]. Available: https://ocw.mit.edu/courses/physics/8-02-physics-ii-electricity-and-magnetism-spring-2007/index.htm

[16] D. C. Meeker, E. H. Maslen, R. C. Ritter, and F. M. Creighton, "Optimal realization of arbitrary forces in a magnetic stereotaxis system," IEEE Trans. on Magnetics, vol. 32, no. 2, pp. 320–328, 1996.

[17] J. J. Abbott, O. Ergeneman, M. P. Kummer, A. M. Hirt, and B. J. Nelson, "Modeling magnetic torque and force for controlled manipulation of soft-magnetic bodies," IEEE Trans. on Robotics, vol. 23, no. 6, pp. 1247–1252, 2007.

[18] S. Das, E. B. Steager, M. A. Hsieh, K. J. Stebe, and V. Kumar, "Experiments and open-loop control of multiple catalytic microrobots," Journal of Micro-Bio Robotics, vol. 14, no. 1-2, pp. 25–34, 2018.

[19] H. E. Nusse and J. A. Yorke, "A procedure for finding numerical trajectories on chaotic saddles," Physica D: Nonlinear Phenomena, vol. 36, no. 1-2, pp. 137–156, 1989.

[20] S. C. Shadden, F. Lekien, and J. E. Marsden, "Definition and properties of lagrangian coherent structures from finite-time lyapunov exponents in two-dimensional aperiodic flows," Physica D: Nonlinear Phenomena, vol. 212, no. 3-4, pp. 271–304, 2005.

[21] B. Krauskopf, H. M. Osinga, E. J. Doedel, M. E. Henderson, J. Guckenheimer, A. Vladimirsky, M. Dellnitz, and O. Junge, "A survey of methods for computing (un) stable manifolds of vector fields," in Modeling And Computations In Dynamical Systems: In Commemoration of the 100th Anniversary of the Birth of John von Neumann. World Scientific, 2006, pp. 67–95.

[22] J. J. Abbott, K. E. Peyer, M. C. Lagomarsino, L. Zhang, L. Dong, I. K. Kaliakatsos, and B. J. Nelson, "How should microrobots swim?" The international journal of Robotics Research, vol. 28, no. 11-12, pp. 1434–1447, 2009.

[23] Itseez, "Open source computer vision library," https://github.com/itseez/opencv, 2015.